

Robust Self-calibration of Focal Lengths from the Fundamental Matrix

Viktor Kocur^{1,2} Daniel Kyselica¹ Zuzana Kúkelová²

¹ Faculty of Mathematics, Physics and Informatics, Comenius University in Bratislava

² Visual Recognition Group, Faculty of Electrical Engineering, Czech Technical University in Prague

{viktor.kocur, daniel.kyselica}@fmph.uniba.sk kukelzuz@fel.cvut.cz

Abstract

The problem of self-calibration of two cameras from a given fundamental matrix is one of the basic problems in geometric computer vision. Under the assumption of known principal points and square pixels, the well-known Bougnoux formula offers a means to compute the two unknown focal lengths. However, in many practical situations, the formula yields inaccurate results due to commonly occurring singularities. Moreover, the estimates are sensitive to noise in the computed fundamental matrix and to the assumed positions of the principal points.

In this paper, we therefore propose an efficient and robust iterative method to estimate the focal lengths along with the principal points of the cameras given a fundamental matrix and priors for the estimated camera parameters. In addition, we study a computationally efficient check of models generated within RANSAC that improves the accuracy of the estimated models while reducing the total computational time. Extensive experiments on real and synthetic data show that our iterative method brings significant improvements in terms of the accuracy of the estimated focal lengths over the Bougnoux formula and other state-of-the-art methods, even when relying on inaccurate priors.

1. Introduction

Camera calibration, *i.e.*, the estimation of camera intrinsic parameters, is a fundamental problem in computer vision with many applications. The precision of estimated intrinsic parameters, such as focal length and principal point, significantly affects the precision of tasks in structure-from-motion (SfM) [38], visual localization [33], 3D object detection [45], augmented reality [6], and other applications [39].

Classical calibration methods [46] use known calibration patterns, *e.g.* checkerboards, or additional knowledge of the observed scene to estimate the camera intrinsics. As such, they are often impractical. On the other hand, self-calibration methods do not require any additional knowledge of the scene geometry and rely on automatic detection

of image features in input cameras. Thus, they are preferable in many applications.

In this paper, we study the problem of self-calibration of two cameras, with potentially different intrinsic parameters that capture the same scene. Although this is a well-studied problem, with first solutions dated back to the nineties, to the best of our knowledge, all its existing solutions suffer from some instabilities and robustness problems.

The geometry of two uncalibrated cameras is captured by the fundamental matrix [28]. In 1998 Bougnoux [2] showed that assuming square pixels and known principal points of both cameras, it is possible to obtain the focal lengths of the two cameras from the fundamental matrix using a closed-form formula. This provides a convenient way to determine the focal length, since the principal point can usually be assumed to lie in the image center. However, the precision of the estimated focal lengths using the Bougnoux formula [2] and other similar methods [10, 18, 29] is often marred by inaccuracies, sometimes even resulting in physically implausible imaginary focal lengths. This stems from singularities and susceptibility of these methods to noise in fundamental matrices and assumed positions of principal points. Moreover, the singularities occur in very common camera configurations when the principal axes of the cameras are coplanar (*i.e.* they intersect), which is common when images of a single object of interest are taken from different views.

An alternative approach [14] relies on iterative optimization of a multiterm loss, allowing one to estimate both the focal lengths of the cameras as well as their principal points. This approach addresses some of the drawbacks of the aforementioned methods but still relies on the Bougnoux formula [2] within the iterative process. It is thus susceptible to inaccuracies, especially in the aforementioned degenerate camera configurations.

Similarly to [14], we formulate the problem of estimating focal lengths and principal points from a given fundamental matrix as a constrained optimization problem using priors. Constraints ensure that the solution satisfies the Kruppa equations [27]. To solve the constrained optimization problem, we search for all stationary points of its La-

grangian. This results in a complex system of polynomial equations that we efficiently solve in an iterative way. Each iteration in our formulation involves solving a system of two polynomial equations of degree four in two variables, which is efficiently solved using the Gröbner basis method [23].

Existing approaches, as well as our method, are based on fundamental matrices that can be estimated using different variants of RANSAC [1, 7–9, 11, 16]. Some of the matrices produced by the 7-point algorithm [15] within RANSAC lead to imaginary focal lengths when decomposed using the Bougnoux formula [2]. We observed that such matrices seldom lead to the final model. Based on this insight, we propose to perform a degeneracy check for such matrices and reject them, thus saving computational time on their further processing, such as scoring and local optimization.

In summary, the contributions of this paper are:

- A novel iterative method for focal length and principal point estimation from fundamental matrices. Evaluation on synthetic and large-scale real-world datasets [17, 47] shows that our method results in superior accuracy of estimated focal lengths as well as camera poses.
- A simple and computationally efficient degeneracy check for fundamental matrices leading to imaginary focal lengths within RANSAC. Performance on real-world datasets [17, 47] shows that performing this check and rejecting such models within various RANSAC variants [1, 7–9] and implementations [3, 16, 24] leads to faster computation and more accurate pose and focal length estimates.

The code for the methods and experiments is available online.¹

2. Related Work

The problem of self-calibration of a camera from a given fundamental matrix is a well-studied problem, with several solutions that can be divided into two main groups, the direct methods and the iterative methods.

2.1. Direct Methods

Bougnoux [2] showed that under the assumption of square pixels and known positions of the principal points, it is possible to calculate the focal lengths of both cameras from the fundamental matrix in closed form. Kanatani and Matsunaga [18] derived a closed form solution directly from the elements of the fundamental matrix, avoiding the intermediate epipole computation required by the Bougnoux formula. Melanitis and Maragos [29] formulated a linear system, the solution of which provides the focal lengths.

These approaches are all algebraically equivalent and thus suffer from the same generic singularity, which occurs whenever the principal axes of the two cameras are coplanar, *i.e.* they are intersecting. This is a very common scenario in practice, as human photographers tend to place objects of interest in the centers of images. The singularity significantly affects the accuracy of the estimated focal lengths even when the axes are close to coplanar.

Similar formulas have been derived for the case when the focal lengths of cameras are known to be equal [4, 18, 41]. In case of equal focal lengths, it is possible to avoid estimating the full 7-DoF fundamental matrix and instead employ a 6-point minimal solver [40] within RANSAC to find the relative poses of cameras along with the focal length. These methods also suffer from generic singularities when the principal axes are parallel, or they intersect, and the camera centers are equidistant from the intersection point [42].

An interesting case is when only one of the focal lengths is unknown. The focal length can be estimated in a closed form solution from the fundamental matrix [44] or using a 6-point minimal solver [5]. A degenerate case for these methods only occurs when the center of the calibrated camera lies on the principal axis of the uncalibrated camera, a situation rarely occurring in practice.

Since focal lengths appear in squared form in the Kruppa equations [27], all the previously mentioned direct methods provide only the squares of focal lengths. This may result in physically implausible imaginary focal lengths due to noise. Depending on the level of noise and camera configuration, imaginary focal lengths may occur at a significant rate (over 20% of samples) [19]. Imaginary focal lengths are less likely to occur when self-calibration is performed using three views [20].

2.2. Iterative Methods

Hartley and Silpa-Anan [14] pointed out that errors in the assumed positions of principal points may significantly affect the focal lengths estimated by the Bougnoux formula. To remedy this issue, they proposed an iterative method based on Levenberg-Marquardt optimization [25]. During the optimization the fundamental matrix, along with the positions of principal points in both images, are optimized to minimize a multiterm loss. The loss consists of the Sampson error on the correspondences and the distance of the principal points and squared focal lengths from predetermined priors. To prevent imaginary focal lengths, the loss also contains a penalization term which dramatically increases the loss whenever the square focal lengths are below a given threshold. During the optimization procedure, the focal lengths are estimated from the fundamental matrix using the Bougnoux formula. This approach overcomes many of the issues of using the formula alone but may still suffer in the vicinity of degenerate camera configurations,

¹https://github.com/kocurvik/robust_self_calibration

as it still relies on the formula to estimate the focal lengths. Additionally, the procedure is computationally expensive as it requires computation of the Sampson error for all correspondences in each iteration.

Iterative methods can also be used to estimate the camera intrinsics using two or more views [10, 12, 27, 31]. When considering only two views with two unknown focal lengths, these methods should converge to the Bougnoux formula. However, these methods may result in different outcomes in the vicinity of degenerate configurations. For example, the method by Fetzer *et al.* [10] optimizes for an energy functional based on the Kruppa equations [27]. In degenerate configurations, the functional does not have a single minimum, yet the optimization procedure will be terminated at some point, providing an output different from the one provided by the Bougnoux formula.

Next, we describe the proposed iterative method that aims to avoid the aforementioned problems of existing approaches for self-calibration from the fundamental matrix.

3. Robust focal length estimation

In this paper, similar to Hartley [14], we formulate the problem of estimating focal lengths from a given fundamental matrix \mathbf{F} as an optimization problem using priors.

Let $\mathbf{F} = \mathbf{UDV}^\top$ be the SVD of the fundamental matrix \mathbf{F} , where $\mathbf{U} = [\mathbf{u}_1, \mathbf{u}_2, \mathbf{u}_3]$ and $\mathbf{V} = [\mathbf{v}_1, \mathbf{v}_2, \mathbf{v}_3]$ are orthonormal matrices and $\mathbf{D} = \text{diag}(\sigma_1, \sigma_2, 0)$ is a diagonal matrix with two non-zero singular values σ_1 and σ_2 of \mathbf{F} . Let $\omega_i^* = \mathbf{K}_i \mathbf{K}_i^\top$ be the dual image of the absolute conic for the i^{th} camera, $i = 1, 2$, with \mathbf{K}_i being the 3×3 calibration matrix of the form

$$\mathbf{K}_i = \begin{bmatrix} f_i & 0 & u_i \\ 0 & f_i & v_i \\ 0 & 0 & 1 \end{bmatrix}, \quad (1)$$

with the focal length f_i and principal point $\mathbf{c}_i = [u_i, v_i]^\top$.

For fixed principal points, *e.g.*, $\mathbf{c}_i = [0, 0]$, $i = 1, 2$, there is a closed form solution for the focal lengths extracted from the given fundamental matrix \mathbf{F} , *i.e.*, the Bougnoux formula [2]. Since this formula can result in unstable or imaginary estimates, in our formulation, we allow moving the estimated principal points to avoid such instabilities. For non-fixed principal points \mathbf{c}_i , there are infinitely many decompositions of \mathbf{F} into the essential matrix \mathbf{E} and two calibration matrices of the form (1). Thus, we formulate the problem of estimating focal lengths from \mathbf{F} as a constrained optimization, where during the optimization, the focal lengths, along with the positions of principal points in both images

are optimized to minimize the following cost function:

$$\begin{aligned} \min_{f_1, f_2, \mathbf{c}_1, \mathbf{c}_2} \quad & \sum_{i=1,2} w_i^f (f_i - f_i^p)^2 + w_i^c \|\mathbf{c}_i - \mathbf{c}_i^p\|^2 \\ \text{s.t.} \quad & \kappa_1 = \sigma_1(\mathbf{v}_1^\top \omega_1^* \mathbf{v}_1)(\mathbf{u}_1^\top \omega_2^* \mathbf{u}_2) + \\ & + \sigma_2(\mathbf{v}_1^\top \omega_1^* \mathbf{v}_2)(\mathbf{u}_2^\top \omega_2^* \mathbf{u}_2) = 0 \\ & \kappa_2 = \sigma_1(\mathbf{v}_1^\top \omega_1^* \mathbf{v}_2)(\mathbf{u}_1^\top \omega_2^* \mathbf{u}_1) + \\ & + \sigma_2(\mathbf{v}_2^\top \omega_1^* \mathbf{v}_2)(\mathbf{u}_1^\top \omega_2^* \mathbf{u}_2) = 0, \end{aligned} \quad (2)$$

where f_i^p and $\mathbf{c}_i^p = [u_i^p, v_i^p]^\top$, $i = 1, 2$ are the priors for the focal lengths and the principal points, w_i^f and w_i^c are predetermined weights, and $\kappa_1 = 0$ and $\kappa_2 = 0$ are two Kruppa equations [27]², which are functions of both focal lengths and principal points that appear in $\omega_i^* = \mathbf{K}_i \mathbf{K}_i^\top$. The Kruppa equations ensure that for the input fundamental matrix \mathbf{F} and the estimated calibration matrices \mathbf{K}_1 and \mathbf{K}_2 (1), the matrix $\mathbf{K}_1^\top \mathbf{F} \mathbf{K}_2$ is a valid essential matrix.

The cost function in (2) has several advantages over the cost function used in [14]. (1) It does not contain a term with the Sampson error on correspondences, which significantly slows down the optimization in [14]. (2) It operates directly on focal lengths f_i instead of squared focal lengths f_i^2 . (3) The minimization of (2) does not require computation or initialization using the Bougnoux formula [2] as used in [14]. Such an initialization can be very far from the ground truth focal lengths and in many scenarios can result in $f_i^2 \leq 0$. Therefore, minimization of (2) does not need a special penalty term for $f_i^2 \leq 0$ as used in [14].

The constrained optimization problem (2) can be transformed into an unconstrained problem using the method of Lagrange multipliers. In this case, this leads to the Lagrange function $L(f_1, f_2, \mathbf{c}_1, \mathbf{c}_2, \lambda_1, \lambda_2)$:

$$L = \sum_{i=1,2} w_i^f (f_i - f_i^p)^2 + w_i^c \|\mathbf{c}_i - \mathbf{c}_i^p\|^2 - 2\lambda_1 \kappa_1 - 2\lambda_2 \kappa_2, \quad (3)$$

where λ_1 and λ_2 are the Lagrange multipliers. The constant ‘ -2 ’ is introduced for easier subsequent manipulation of the equations and it does not influence the final solution.

In this case, if $(f_1^*, f_2^*, \mathbf{c}_1^*, \mathbf{c}_2^*)$ is a point of the minimum of the original constrained problem (2), then there exists λ_1^* and λ_2^* such that $(f_1^*, f_2^*, \mathbf{c}_1^*, \mathbf{c}_2^*, \lambda_1^*, \lambda_2^*)$ is a stationary point of L (3), *i.e.*, a point where all the partial derivatives of L vanish. The Lagrange function $L(f_1, f_2, \mathbf{c}_1, \mathbf{c}_2, \lambda_1, \lambda_2)$ (3) is a function of eight unknowns. Thus, to find all stationary points of L we need to solve the following system of eight

²Note, that there are three Kruppa equations, but only two are linearly independent.

polynomial equations in eight unknowns ³:

$$2w_i^f(f_i - f_i^p) - 2\lambda_1 \frac{\partial \kappa_1}{\partial f_i} - 2\lambda_2 \frac{\partial \kappa_2}{\partial f_i} = 0, \quad (4)$$

$$2w_i^c(\mathbf{c}_i - \mathbf{c}_i^p) - 2\lambda_1 \left(\frac{\partial \kappa_1}{\partial \mathbf{c}_i} \right)^\top - 2\lambda_2 \left(\frac{\partial \kappa_2}{\partial \mathbf{c}_i} \right)^\top = \mathbf{0}, \quad (5)$$

$$\kappa_1 = 0, \quad (6)$$

$$\kappa_2 = 0. \quad (7)$$

Unfortunately, the system of eight equations (4)–(7) is too complex to be efficiently solved using an algebraic method, *e.g.* using the Gröbner basis method [21, 23]. Next, we propose an iterative method to efficiently solve this system of polynomial equations. Note that in our method, we estimate all stationary points of the Lagrange function L (3). Thus, we avoid potential problems of numerical methods that directly minimize (3). Such methods usually require good initialization and can get stuck in local minima.

3.1. Iterative method

First, let us denote $\Delta f_i = f_i - f_i^p$, $\Delta \mathbf{c}_i = \mathbf{c}_i - \mathbf{c}_i^p$, $i = 1, 2$. From equations (4)–(5) we have

$$\Delta f_i = \frac{1}{w_i^f} \left(\lambda_1 \frac{\partial \kappa_1}{\partial f_i} + \lambda_2 \frac{\partial \kappa_2}{\partial f_i} \right), \quad (8)$$

$$\Delta \mathbf{c}_i = \frac{1}{w_i^c} \left(\lambda_1 \left(\frac{\partial \kappa_1}{\partial \mathbf{c}_i} \right)^\top + \lambda_2 \left(\frac{\partial \kappa_2}{\partial \mathbf{c}_i} \right)^\top \right). \quad (9)$$

and the cost function in the original constrained optimization problem (2) can be rewritten as

$$e = \sum_{i=1,2} w_i^f \Delta f_i^2 + w_i^c \Delta \mathbf{c}_i^\top \Delta \mathbf{c}_i \quad (10)$$

The proposed iterative solution to equations (4)–(7) follows the idea of iterative triangulation methods [22, 26]. First, let $s^{k-1} = \langle f_1^{k-1}, f_2^{k-1}, \mathbf{c}_1^{k-1}, \mathbf{c}_2^{k-1} \rangle$ denote the best current estimate of focal lengths and principal points after the $(k-1)^{th}$ iteration. The prior values $f_i^0 \equiv f_i^p$, $\mathbf{c}_i^0 \equiv \mathbf{c}_i^p$, $i = 1, 2$ are used as an initialization. In the k^{th} iteration the updated estimates $s^k = \langle f_1^k, f_2^k, \mathbf{c}_1^k, \mathbf{c}_2^k \rangle$ are obtained by replacing the focal lengths and principal points $\langle f_1, f_2, \mathbf{c}_1, \mathbf{c}_2 \rangle$ on the right-hand side of equations (8)–(9) by the current best estimates $s^{k-1} = \langle f_1^{k-1}, f_2^{k-1}, \mathbf{c}_1^{k-1}, \mathbf{c}_2^{k-1} \rangle$. In this way, we obtain the expressions for $\Delta f_i = \frac{1}{w_i^f} (\lambda_1 \frac{\partial \kappa_1}{\partial f_i}(s^{k-1}) + \lambda_2 \frac{\partial \kappa_2}{\partial f_i}(s^{k-1}))$ and $\Delta \mathbf{c}_i = \frac{1}{w_i^c} (\lambda_1 (\frac{\partial \kappa_1}{\partial \mathbf{c}_i}(s^{k-1}))^\top + \lambda_2 (\frac{\partial \kappa_2}{\partial \mathbf{c}_i}(s^{k-1}))^\top)$, $i = 1, 2$. Here $\frac{\partial \kappa_j}{\partial f_i}(s^{k-1})$ and $\frac{\partial \kappa_j}{\partial \mathbf{c}_i}(s^{k-1})$, $i, j = 1, 2$ are partial derivatives of κ_j evaluated at $s^{k-1} = \langle f_1^{k-1}, f_2^{k-1}, \mathbf{c}_1^{k-1}, \mathbf{c}_2^{k-1} \rangle$. After this substitution, Δf_i and $\Delta \mathbf{c}_i$ are functions of two Lagrange multipliers λ_1 and λ_2 .

³Note that (4) represents two equations for $i = 1, 2$ and (5) represents four equations since there are two vector equations for $i = 1, 2$.

Expressions Δf_i and $\Delta \mathbf{c}_i$ are, in turn, substituted into the Kruppa equations (6) and (7). This is done by substituting Δf_i and $\Delta \mathbf{c}_i$, $i = 1, 2$ into ω_i^* using the relationship $f_i = \Delta f_i + f_i^p$ and $\mathbf{c}_i = \Delta \mathbf{c}_i + \mathbf{c}_i^p$.

The updated Kruppa equations (6) and (7), which we denote $\kappa_1^k = 0$ and $\kappa_2^k = 0$, form a system of two equations of degree four in two unknowns λ_1 and λ_2 . This system has up to 16 real solutions and can be efficiently solved using the Gröbner basis method [23]. The final solver performs an elimination of a 20×36 matrix and extracts solutions from the eigenvalues and eigenvectors of a 16×16 matrix.

From up to 16 possible solutions, a solution λ_1^k and λ_2^k that minimizes $|\lambda_1| + |\lambda_2|$ is selected [26]. This solution is used to compute the k^{th} iteration updates Δf_i^k and $\Delta \mathbf{c}_i^k$ using equations (8)–(9) and subsequently the new estimates of focal lengths and principal points $s^k = \langle f_1^k, f_2^k, \mathbf{c}_1^k, \mathbf{c}_2^k \rangle$.

The iterative algorithm stops when the relative change of error of two consecutive iterations $\frac{|e^k - e^{k-1}|}{e^k} < \epsilon$, for some threshold ϵ . Note that in each iteration, the obtained solutions satisfy the Kruppa equations $\kappa_1 = 0$ and $\kappa_2 = 0$. This means that for the input fundamental matrix \mathbf{F} and the estimated calibration matrices \mathbf{K}_1 and \mathbf{K}_2 (1), the matrix $\mathbf{K}_1^\top \mathbf{F} \mathbf{K}_2$ is a valid essential matrix in each iteration.

The situation with $f_1 = f_2$ can be solved using the same method. In this case, in the cost function (2), as well as in the Lagrangian and in (4)–(5), we only have $i = 1$. However, since we still have two Kruppa equations $\kappa_1 = 0$ and $\kappa_2 = 0$ the final algorithm also relies on solutions to a system of two equations of degree four in two unknowns. The algorithm is summarized in the Supplementary material.

3.2. Real Focal Length Checking within RANSAC

The method proposed in 3.1 is usually applied on a fundamental matrix \mathbf{F} that is obtained using a robust RANSAC-style estimation [1, 7–9, 11, 16]. Compared to the Bougnoux formula [2], our method does not suffer from imaginary focal length estimates in the presence of noise or an error in the principal point location. Thus, our method does not need to check whether the fundamental matrix returned by the RANSAC is decomposable to real focal lengths or not. Nevertheless, as we observed in our experiments, fundamental matrices that result in imaginary focal lengths usually do not provide good estimates and are therefore not selected inside RANSAC as best models.

Inspired by this observation, we propose a simple modification of RANSAC that is based on rejecting models that lead to imaginary focal lengths. Rejection is done before scoring models on all point correspondences. This reduces the computational time required to score a model, which is unlikely to lead to the final output. Thus, this approach is similar to other degeneracy checking algorithms.

To reject models, we use a modified version of the Bougnoux formula [2] presented in [32], which has the form of a

ratio of two polynomials in the elements of the fundamental matrix. The formula returns squared focal lengths. When the sign of one of the squared focal lengths is negative, we reject the model. This approach does not require the use of SVD or other expensive matrix manipulations. This type of checking can be implemented into different variants of RANSACs and, as shown later in our experiments, it leads to reduced computational times while maintaining or even improving accuracy of pose estimates. Implementation details can be found in the Supplementary Material (SM).

4. Synthetic Experiments

We perform several synthetic experiments to evaluate various aspects of our method and compare it with the state-of-the-art in controlled configurations. Here, we only include experiments for two unknown but different focal lengths. Further experiments for the case where the focal lengths are assumed to be equal can be found in the SM.

In all our synthetic and real experiments, we set the weights in (2) to $w_i^f = 5 \cdot 10^{-4}$ and $w_i^c = 1.0$. These weights were obtained by testing different combinations on the Brandenburg Gate validation scene from the Phototurism dataset [17] and resulted in the best performance on this scene. However, as we show also in synthetic experiments, for a wide variety of combinations of weights, we consistently obtain very good estimates and outperform the state-of-the-art methods. We set the weights for Hartley and Silpa-Anan's method [14] in the same manner to 1.0 for w_F , 10^{-4} for w_c and 10^{-6} for w_f .

Camera Setup: To perform the experiments, we set up a scene with two cameras. We assume 640×480 image size and principal points in image centers. The first camera has focal length $f_1 = 600$ and the second $f_2 = 400$. The first camera has center at the origin with the z-axis of the world coordinate system being its principal axis. We perform experiments with the second camera in different configurations denoted as $\mathcal{C}(\theta, y)$. For $\mathcal{C}(0^\circ, y)$ the second camera center is located at coordinates $(1200, y, 600)$. The camera is rotated by 60° around its y -axis. With $\theta \neq 0^\circ$ we additionally rotate the second camera around the x -axis by θ . When $y = 0$ and $\theta = 0^\circ$ the principal axes of the two cameras intersect and are thus coplanar, which is a degenerate configuration for the Bougnoux formula [2].

For a given camera setup, we uniformly generate 100 random points visible by both cameras. After projecting the points into both images, we add Gaussian noise with a standard deviation σ_n to the pixel coordinates. We also emulate errors in the assumed locations of the principal points. The principal points are shifted from the image centers by a distance sampled from the normal distribution with a standard deviation of σ_p . We estimate the fundamental matrix using MAGSAC++ [1] as implemented in OpenCV [3].

Convergence: In the first experiment, we evaluate convergence of the proposed iterative method. Different termination criteria can be considered. We terminate the algorithm when the relative change in error in two successive iterations $\frac{|e^n - e^{n-1}|}{e^n}$ is less than a predetermined threshold. Fig. 1a shows that for non-degenerate configuration our method converges quickly even with strict thresholds. Fig. 1b shows the convergence rates of our method when the principal axes are coplanar. The degenerate configuration requires an increased number of iterations to converge with the same thresholds. However, even in a degenerate configuration, the method converges in a few iterations for most of the samples, even with strict thresholds. We also evaluate convergence on a large scale real-world dataset [17] (see section 5 for more details). As shown in Fig. 1c, our method successfully converges for most of the samples even with a strict threshold. Using these findings, we established the maximum number of iterations for our method at 50, as further iterations demonstrated diminishing returns in terms of convergence rate.

Accuracy of the Estimated Focal Lengths In the next experiment, we compare our method with state-of-the-art methods in terms of accuracy of the estimated focal lengths. The methods considered are the baseline Bougnoux formula [2] and the iterative approaches of Hartley and Silpa-Anan [14] and Fetzer *et al.* [10]. In the experiments, we use the same priors for Hartley and Silpa-Anan's method as for ours. We set the initial values for LM optimization for the method by Fetzer *et al.* to the same values as our priors.

Fig. 2a and 2b show how the transition to a degenerate configuration with coplanar principal axes affects the accuracy of the evaluated methods. Our method performs well even close to and in degenerate configurations. In comparison, the other evaluated methods fail to provide consistent results when the camera position approaches the degenerate configuration.

A similar trend is visible in Fig. 2c where we show that an increase in the difference between the assumed and ground truth position of the principal point results in a worsening performance of the Bougnoux formula and the method by Fetzer *et al.* Our method is capable of compensating for the error in the principal point as the principal point is not assumed to be known exactly. The performance of Hartley and Silpa-Anan's method stays consistent for similar reasons, although it performs worse than ours.

In Fig. 2d, we show the performance of the methods under varying levels of added image noise. Our method demonstrates a higher robustness to noise, resulting in reduced inter-sample deviation and a more consistent median estimate across the various noise levels. Fig. 2e shows how the different methods respond to the priors for focal length, or in the case of the method by Fetzer *et al.* to an initializa-

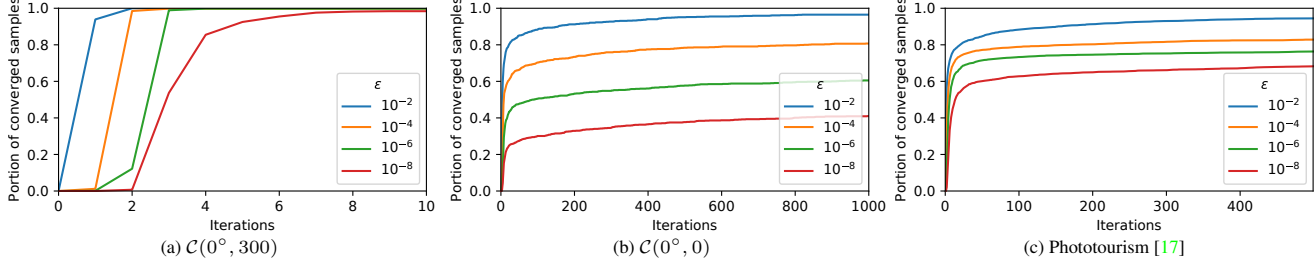


Figure 1. Plots showing portion of samples for which our algorithm would converge given a threshold for the relative change of errors in successive iterations $\frac{|e^n - e^{n-1}|}{e^n} < \epsilon$. For synthetic experiments (a) and (b) we generated 1000 samples with added noise ($\sigma_n = 1$, $\sigma_p = 10$). We set the priors as $f_1^p = 660$, $f_2^p = 440$. For (c) we used the Phototourism benchmark dataset [17]. See Section 5 for details.

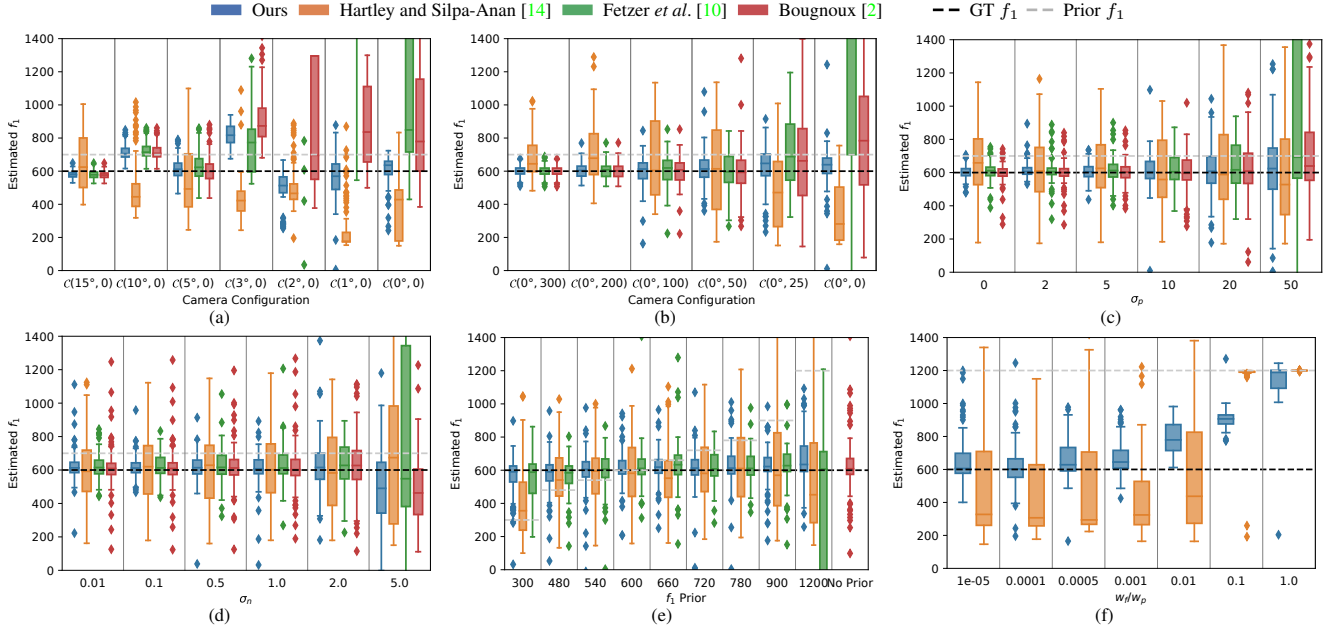


Figure 2. Synthetic experiments: Box plots for the estimated focal lengths of the first camera. Comparison of the methods as (a, b) the camera configuration approaches the degeneracy with coplanar principal axes, (c) we vary the standard deviation σ_p of the error of the principal point, (d) we vary the noise added to the projected points, (e) we vary the prior for f_1 , (f) we vary the relative weights of focal length and principal point priors. We use priors $f_1^p = 700$, $f_2^p = 400$ for (a, b, c, d), $f_1^p = 1000$, $f_2^p = 400$ for (f), $\sigma_n = 1$ for (a, b, c, d, e, f), $\sigma_p = 10$ for (a, b, d, e, f). For (c, d, e, f) we randomly sample the configuration $\mathcal{C}(\theta, y)$ with $\theta \in [-15^\circ, 15^\circ]$ and $y \in [-200, 200]$.

tion for the iterative process. Fig. 2f shows how the setting of weights for our and Hartley and Silpa-Anan's method affects the accuracy of the estimated focal lengths.

5. Real-world Experiments

Datasets: We assess the real-world performance of our method using two extensive datasets. The first dataset, referred to as the **Phototourism dataset**, was originally introduced in [17] to serve as a robust benchmark to evaluate structure-from-motion pipelines. The dataset contains 25 scenes of landmarks. Large sets of crowd-sourced images are available for each scene. For 13^4 of the scenes

⁴Originally, reconstructions were available for 16 of the scenes, but 3 of the scenes were later dropped from the dataset due to data inconsistencies.

a COLMAP [36] reconstruction is provided to serve as ground truth for camera intrinsics and extrinsics. To evaluate the estimated focal lengths, we randomly sample 1000 pairs of images for each scene. We only consider pairs with sufficient co-visibility as defined in [17]. We used the Brandenburg Gate scene to serve as a validation set to determine the optimal setting of the weights w_i^f and w_i^c in (2).

The second dataset, known as the **Aachen Day-Night v1.1 Dataset**, is an extension of the previously established Aachen Day-Night dataset [34, 35]. This dataset incorporates a reference COLMAP [36] model that has been reconstructed from a comprehensive collection of 6,697 images captured by a variety of cameras and smartphones. For evaluation, we randomly sample 1000 pairs of images that

Method	RFC	Phototourism [17]						Aachen Day-Night v1.1 [47]					
		Median p_{err}	mAA _p		Median f_{err}	mAA _f		Median p_{err}	mAA _p		Median f_{err}	mAA _f	
			10°	20°		0.1	0.2		10°	20°		0.1	0.2
Ours	✓	6.43° 6.29°	40.48 41.03	56.01 56.78	0.146 0.143	24.15 24.47	37.72 38.19	9.52° 8.78°	27.62 29.29	46.28 48.13	0.199 0.188	12.61 13.20	25.59 27.33
Hartley [14]	✓	9.19° 9.00°	30.15 30.61	46.94 47.69	0.215 0.211	13.35 13.49	25.45 25.76	12.19° 11.37°	21.10 22.12	38.74 40.61	0.263 0.245	6.77 7.66	14.94 16.55
Fetzer [10]	✓	9.40° 8.94°	33.00 33.64	47.25 48.51	0.218 0.204	19.97 20.38	30.84 31.62	12.33° 10.66°	24.34 25.62	39.69 42.16	0.251 0.226	12.07 12.16	23.62 24.84
Bougnoux [2]	✓	7.55° 7.39°	37.17 37.57	52.70 53.21	0.197 0.187	21.09 21.51	32.44 33.25	10.25° 9.69°	26.73 27.25	45.07 45.61	0.250 0.223	11.96 12.44	23.72 25.17
Prior	✓	11.17° 11.05°	22.63 22.73	41.98 42.31	0.206 0.206	9.52 9.52	22.75 22.75	13.00° 12.73°	17.06 17.68	37.27 38.05	0.195 0.195	4.43 4.43	10.02 10.02
GT intrinsics	✓	2.85° 2.82°	59.78 60.05	70.80 71.18	—	—	—	5.45° 4.25°	45.99 51.76	58.66 64.82	—	—	—

Table 1. Median errors for poses (p_{err}) and focal lengths (f_{err}) and mean average accuracy scores for poses (mAA_p) and estimated focal lengths (mAA_f) on 12 scenes from the Phototourism dataset [17] and the Aachen Day-Night v1.1 dataset [47]. RFC denotes real focal length checking as described in subsection 3.2.

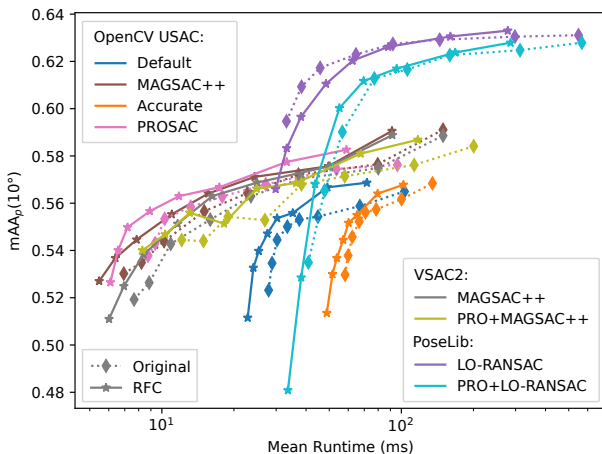


Figure 3. The plot shows mAA_p achieved on the Phototourism dataset [17] for different RANSAC implementations [3, 16, 24] with and without real focal length checking (RFC) under varying number of iterations. To calculate the poses we use the ground truth focal lengths. Further details are provided in the SM.

adhere to the same co-visibility criteria as those defined for the Phototourism dataset.

Fundamental Matrix Estimation: We use LoFTR [43] to obtain point correspondences. We perform inference on images resized so that the largest dimension is equal to 1024 px. To estimate the fundamental matrix, we use MAGSAC++ [1] with the epipolar threshold set to 3 px.

We also perform experiments with and without utilizing real focal length checking (RFC) as described in subsection 3.2. Fig 3 shows that on the Phototourism dataset [17] the fundamental matrices obtained with RFC generally lead to more accurate pose estimates while also significantly reducing computational times across various RANSAC im-

plementations. Implementation details and further experiments are provided in SM.

Compared Methods: We compare our method with three state-of-the-art approaches. We evaluate the Bougnoux formula [2], Hartley and Silpa-Anan’s iterative method [14] and the iterative method by Fetzer *et al.* [10].

For all images, we consider the principal point to lie in their center which is a commonly used assumption. With the exception of the Bougnoux formula, all methods require priors, or initial estimates, for the focal lengths. Following common practice, as established in COLMAP [36], we initialize the priors for focal lengths at 1.2 times the maximum dimension of the image (i.e., either width or height). This initial setting implies an approximate 50-degree field of view for the cameras.

Metrics: To evaluate the accuracy of the output focal lengths, we define relative focal length error as

$$f_{err} = \frac{|f_i^{est} - f_i^{gt}|}{\max(f_i^{est}, f_i^{gt})}, \quad (11)$$

with f_i^{est} and f_i^{gt} denoting the estimated and ground truth focal lengths respectively, with $i \in \{1, 2\}$ denoting the first or the second camera. To gauge the accuracy of the poses, we employ the Mean Average Accuracy (mAA) metric, as originally proposed in [17]. The basis for this metric is the pose error (p_{err}) which is calculated as the maximum of the rotation and translation error in degrees.

Furthermore, we employ the mAA metric to evaluate and compare the accuracy of the estimated focal lengths, based on the f_i^{err} curves as presented in Figure 4. To distinguish between the two applications of the mAA metric, we denote them as mAA_p for pose and mAA_f for focal lengths.

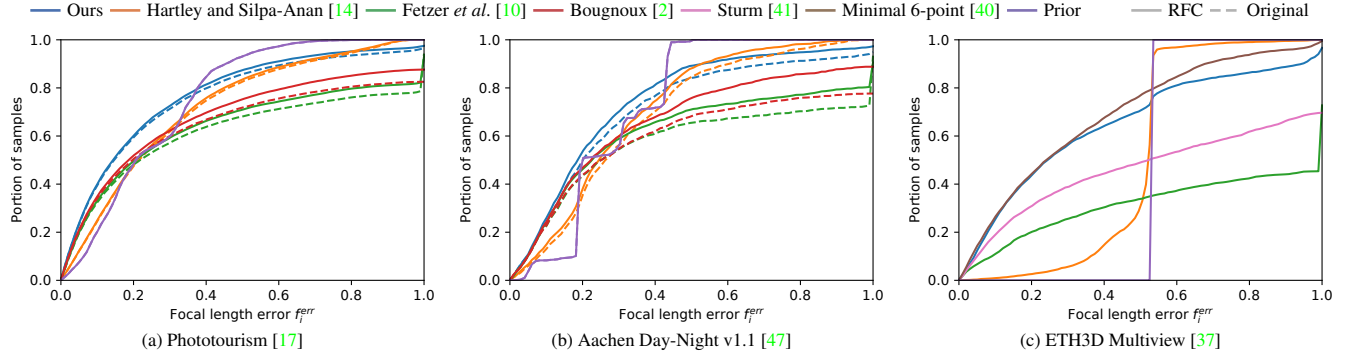


Figure 4. Plots showing the portion of samples for which the estimated focal lengths were below a given f_i^err threshold. For (a) and (b) we assume different focal lengths for the two cameras, for (c) the focal lengths are assumed to be equal.

Method	Library	RFC	Mean Time (ms)	Mean iterations
Ours	Matlab	✓	22.42	24.33
			14.95	22.53
	Eigen (C++)	✓	3.59	23.63
			3.44	22.49
Hartley [14]	PyTorch [30]	✓	659.61	85.38
			663.98	86.14
Fetzer [10]	PyTorch [30]	✓	197.89	0.00
			191.75	40.56
Bougnoux [2]	NumPy [13]	✓	0.27	—
			0.25	—

Table 2. Mean computation times and number of iterations for the compared methods on the Phototourism dataset [17]. Measurements were performed on Intel i7-11800H. The times shown do not include the estimation of the fundamental matrices.

Results: The median errors and mean average accuracy scores for both pose and focal lengths are reported in Table 1. On both the Phototourism and the Aachen dataset, our method significantly outperforms others in terms of the accuracy of the estimated focal lengths. The superiority of our method in terms of focal length accuracy can also be seen in Fig. 4a and 4b. In terms of pose accuracy, our method also provides more accurate results than all compared methods.

The results also show that performing RFC for real focal lengths within RANSAC as proposed in subsection 3.2 generally leads to improvements in terms of both the pose and focal length accuracy across the compared methods.

Computational Speed: Table 2 shows the mean computational times for the various methods. Our method is significantly faster than other iterative methods. Note that the implementation of our method is not optimized and there is still some space for speed-up.

Equal Focal Lengths: We also evaluate our method for the case when both focal lengths can be assumed to be equal. In this case, we use the modified version of our iterative algorithm from Section 3.1. To perform the evaluation, we use the ETH3D Multiview dataset [37]. We use all image pairs satisfying the co-visibility criterion for each

Method	Median p_{err}	mAA _p		Median f_{err}	mAA _f	
		10°	20°		0.1	0.2
Ours	16.50°	16.70	32.24	0.244	13.69	25.01
Hartley [14]	21.51°	12.38	24.26	0.523	0.46	1.12
Fetzer [10]	70.40°	2.31	5.20	0.999	6.86	11.64
Sturm [41]	17.98°	20.64	33.30	0.524	10.78	18.46
Minimal [40]	36.18°	16.42	25.74	0.239	15.04	25.89
Prior	24.59°	11.24	20.92	0.528	0.00	0.00
GT intrinsics	6.39°	41.73	54.16	—	—	—

Table 3. Mean average accuracy scores for poses (mAA_p) and estimated focal lengths (mAA_f) on 12 scenes from the ETH3D High Resolution Multiview dataset [37]. The focal lengths of both cameras are assumed to be equal. The last row includes reference results for pose accuracy when ground truth intrinsics are used.

of the 12 scenes from the test set, yielding 3830 total pairs. For comparison, we modified the method by Fetzer *et al.* to optimize for a single focal length. We use Hartley and Silpa-Anan’s method as usual, but on output we average the two focal lengths produced. Instead of the Bougnoux formula, we use the formula proposed by Sturm [41] which is specific to the case of equal focal lengths. We also evaluate the minimal 6-point algorithm [40] implemented within LO-RANSAC [8, 24]. Further details and additional experiments are available in SM.

The results are shown in Table 3 and Fig. 4c. Our method provides superior results to other methods based on the decomposition of the fundamental matrix, and performs comparably to the approach based on the minimal solver [40] in terms of estimated focal lengths and shows minor improvements in terms of pose accuracy. Our method thus provides a good alternative to the 6-point minimal solver in the case when the focal lengths of the two cameras are known to be equal.

6. Conclusion

We address the important problem of robust self-calibration of the focal lengths of two cameras from a given

fundamental matrix. Our new efficient iterative method shows substantial improvements over existing techniques. Synthetic experiments show that our method performs reliably even when the cameras are in or close to degenerate configurations. In real-world evaluations on two large-scale datasets, our approach demonstrates superior accuracy in terms of estimated poses and focal lengths, even when we use inaccurate initial priors, while also being faster than competing iterative approaches.

We have additionally proposed to perform a computationally simple check within the standard 7-point algorithm to remove models that lead to imaginary focal lengths. Real-world experiments show that this approach not only decreases computational time of the whole RANSAC pipeline, but, in general, also leads to improved pose and focal length accuracy across multiple RANASC variants and implementations.

References

- [1] Daniel Barath, Jana Noskova, Maksym Ivashechkin, and Jiri Matas. Magsac++, a fast, reliable and accurate robust estimator. In *Proceedings of the IEEE/CVF conference on computer vision and pattern recognition*, pages 1304–1312, 2020. [2](#), [4](#), [5](#), [7](#)
- [2] Sylvain Bougnoux. From projective to euclidean space under any practical situation, a criticism of self-calibration. In *Sixth International Conference on Computer Vision*, pages 790–796. IEEE, 1998. [1](#), [2](#), [3](#), [4](#), [5](#), [6](#), [7](#), [8](#)
- [3] Gary Bradski. The opencv library. *Dr. Dobb’s Journal: Software Tools for the Professional Programmer*, 25(11):120–123, 2000. [2](#), [5](#), [7](#)
- [4] Michael J Brooks, Lourdes de Agapito, Du Q Huynh, and Luis Baumela. Towards robust metric reconstruction via a dynamic uncalibrated stereo head. *Image and Vision Computing*, 16(14):989–1002, 1998. [2](#)
- [5] Martin Bujnak, Zuzana Kukelova, and Tomas Pajdla. 3d reconstruction from image collections with a single known focal length. In *2009 IEEE 12th International Conference on Computer Vision*, pages 1803–1810. IEEE, 2009. [2](#)
- [6] Robert Castle, Georg Klein, and David W. Murray. Video-rate localization in multiple maps for wearable augmented reality. In *ISWC*, 2008. [1](#)
- [7] Ondrej Chum and Jiri Matas. Matching with prosac—progressive sample consensus. In *2005 IEEE computer society conference on computer vision and pattern recognition (CVPR’05)*, volume 1, pages 220–226. IEEE, 2005. [2](#), [4](#)
- [8] Ondřej Chum, Jiří Matas, and Josef Kittler. Locally optimized ransac. In *Pattern Recognition: 25th DAGM Symposium, Magdeburg, Germany, September 10-12, 2003. Proceedings 25*, pages 236–243. Springer, 2003. [2](#), [4](#), [8](#)
- [9] Ondrej Chum, Tomas Werner, and Jiri Matas. Two-view geometry estimation unaffected by a dominant plane. In *2005 IEEE Computer Society Conference on Computer Vision and Pattern Recognition (CVPR’05)*, volume 1, pages 772–779. IEEE, 2005. [2](#), [4](#)
- [10] Torben Fetzer, Gerd Reis, and Didier Stricker. Stable intrinsic auto-calibration from fundamental matrices of devices with uncorrelated camera parameters. In *Proceedings of the IEEE/CVF Winter Conference on Applications of Computer Vision*, pages 221–230, 2020. [1](#), [3](#), [5](#), [6](#), [7](#), [8](#)
- [11] Martin A Fischler and Robert C Bolles. Random sample consensus: a paradigm for model fitting with applications to image analysis and automated cartography. *Communications of the ACM*, 24(6):381–395, 1981. [2](#), [4](#)
- [12] Riccardo Gherardi and Andrea Fusiello. Practical autocalibration. In *Computer Vision–ECCV 2010: 11th European Conference on Computer Vision, Heraklion, Crete, Greece, September 5–11, 2010, Proceedings, Part I 11*, pages 790–801. Springer, 2010. [3](#)
- [13] Charles R. Harris, K. Jarrod Millman, Stéfan J. van der Walt, Ralf Gommers, Pauli Virtanen, David Cournapeau, Eric Wieser, Julian Taylor, Sebastian Berg, Nathaniel J. Smith, Robert Kern, Matti Picus, Stephan Hoyer, Marten H. van Kerkwijk, Matthew Brett, Allan Haldane, Jaime Fernández del Río, Mark Wiebe, Pearu Peterson, Pierre Gérard-Marchant, Kevin Sheppard, Tyler Reddy, Warren Weckesser, Hameer Abbasi, Christoph Gohlke, and Travis E. Oliphant. Array programming with NumPy. *Nature*, 585(7825):357–362, Sept. 2020. [8](#)
- [14] Richard Hartley, Chanop Silpa-Anan, et al. Reconstruction from two views using approximate calibration. In *Proc. 5th Asian Conf. Comput. Vision*, volume 1, pages 338–343, 2002. [1](#), [2](#), [3](#), [5](#), [6](#), [7](#), [8](#)
- [15] R. Hartley and A. Zisserman. *Multiple View Geometry in Computer Vision*. Cambridge, 2nd edition, 2003. [2](#)
- [16] Maksym Ivashechkin, Daniel Barath, and Jiří Matas. Vsac: Efficient and accurate estimator for h and f. In *Proceedings of the IEEE/CVF international conference on computer vision*, pages 15243–15252, 2021. [2](#), [4](#), [7](#)
- [17] Yuhe Jin, Dmytro Mishkin, Anastasiia Mishchuk, Jiri Matas, Pascal Fua, Kwang Moo Yi, and Eduard Trulls. Image matching across wide baselines: From paper to practice. *International Journal of Computer Vision*, 129(2):517–547, 2021. [2](#), [5](#), [6](#), [7](#), [8](#)
- [18] Kenichi Kanatani and Chikara Matsunaga. Closed-form expression for focal lengths from the fundamental matrix. In *Proc. 4th Asian Conf. Comput. Vision*, volume 1, pages 128–133. Citeseer, 2000. [1](#)
- [19] Kenichi Kanatani, Atsutada Nakatsuji, and Yasuyuki Sugaya. Stabilizing the focal length computation for 3-d reconstruction from two uncalibrated views. *International Journal of Computer Vision*, 66:109–122, 2006. [2](#)
- [20] Yasushi Kanazawa, Yasuyuki Sugaya, and Kenichi Kanatani. Initializing 3-d reconstruction from three views using three fundamental matrices. In *Image and Video Technology-PSIVT 2013 Workshops: GCCV 2013, GPID 2013, PAES-NPR 2013, and QACIVA 2013, Guanajuato, Mexico, October 28–29, 2013, Revised Selected Papers 6*, pages 169–180. Springer, 2014. [2](#)
- [21] Zuzana Kukelova, Martin Bujnak, and Tomas Pajdla. Automatic generator of minimal problem solvers. In *Computer Vision–ECCV 2008: 10th European Conference on Com-*

puter Vision, Marseille, France, October 12-18, 2008, Proceedings, Part III 10, pages 302–315. Springer, 2008. 4

[22] Zuzana Kukelova and Viktor Larsson. Radial distortion triangulation. In *Proceedings of the IEEE/CVF Conference on Computer Vision and Pattern Recognition*, pages 9681–9689, 2019. 4

[23] Viktor Larsson, Kalle Astrom, and Magnus Oskarsson. Efficient solvers for minimal problems by syzygy-based reduction. In *Proceedings of the IEEE Conference on Computer Vision and Pattern Recognition*, pages 820–829, 2017. 2, 4

[24] Viktor Larsson and contributors. PoseLib - Minimal Solvers for Camera Pose Estimation, 2020. 2, 7, 8

[25] Kenneth Levenberg. A method for the solution of certain non-linear problems in least squares. *Quarterly of applied mathematics*, 2(2):164–168, 1944. 2

[26] Peter Lindstrom. Triangulation made easy. In *2010 IEEE Computer Society Conference on Computer Vision and Pattern Recognition*, pages 1554–1561. IEEE, 2010. 4

[27] Manolis IA Lourakis and Rachid Deriche. *Camera self-calibration using the Kruppa equations and the SVD of the fundamental matrix: The case of varying intrinsic parameters*. PhD thesis, INRIA, 2000. 1, 2, 3

[28] Quan-Tuan Luong and Olivier D Faugeras. The fundamental matrix: Theory, algorithms, and stability analysis. *International journal of computer vision*, 17(1):43–75, 1996. 1

[29] Nikos Melanitis and Petros Maragos. A linear method for camera pair self-calibration. *Computer Vision and Image Understanding*, 210:103223, 2021. 1, 2

[30] Adam Paszke, Sam Gross, Francisco Massa, Adam Lerer, James Bradbury, Gregory Chanan, Trevor Killeen, Zeming Lin, Natalia Gimelshein, Luca Antiga, Alban Desmaison, Andreas Kopf, Edward Yang, Zachary DeVito, Martin Raison, Alykhan Tejani, Sasank Chilamkurthy, Benoit Steiner, Lu Fang, Junjie Bai, and Soumith Chintala. Pytorch: An imperative style, high-performance deep learning library. In *Advances in Neural Information Processing Systems* 32, pages 8024–8035. Curran Associates, Inc., 2019. 8

[31] Marc Pollefeys, Reinhard Koch, and Luc Van Gool. Self-calibration and metric reconstruction inspite of varying and unknown intrinsic camera parameters. *International journal of computer vision*, 32(1):7–25, 1999. 3

[32] Oleh Rybkin. Robust focal length estimation. Bachelor’s thesis, Czech Technical University in Prague, 2017. 4

[33] Torsten Sattler, Bastian Leibe, and Leif Kobbelt. Efficient & effective prioritized matching for large-scale image-based localization. *IEEE Trans. Pattern Anal. Mach. Intell.*, 39(9):1744–1756, 2017. 1

[34] Torsten Sattler, Will Maddern, Carl Toft, Akihiko Torii, Lars Hammarstrand, Erik Stenborg, Daniel Safari, Masatoshi Okutomi, Marc Pollefeys, Josef Sivic, Fredrik Kahl, and Tomas Pajdla. Benchmarking 6DOF Outdoor Visual Localization in Changing Conditions. In *Conference on Computer Vision and Pattern Recognition (CVPR)*, 2018. 6

[35] Torsten Sattler, Tobias Weyand, Bastian Leibe, and Leif Kobbelt. Image Retrieval for Image-Based Localization Revisited. In *British Machine Vision Conference (BMVC)*, 2012. 6

[36] Johannes Lutz Schönberger and Jan-Michael Frahm. Structure-from-motion revisited. In *Conference on Computer Vision and Pattern Recognition (CVPR)*, 2016. 6, 7

[37] Thomas Schops, Johannes L Schonberger, Silvano Galliani, Torsten Sattler, Konrad Schindler, Marc Pollefeys, and Andreas Geiger. A multi-view stereo benchmark with high-resolution images and multi-camera videos. In *Proceedings of the IEEE conference on computer vision and pattern recognition*, pages 3260–3269, 2017. 8

[38] Noah Snavely, Steven M Seitz, and Richard Szeliski. Modeling the world from internet photo collections. *IJCV*, 80(2):189–210, 2008. 1

[39] Jakub Sochor, Roman Juránek, Jakub Špařhel, Lukáš Maršík, Adam Široký, Adam Herout, and Pavel Zemčík. Comprehensive data set for automatic single camera visual speed measurement. *IEEE Transactions on Intelligent Transportation Systems*, 20(5):1633–1643, 2018. 1

[40] Henrik Stewénius, David Nistér, Fredrik Kahl, and Fredrik Schaffalitzky. A minimal solution for relative pose with unknown focal length. *Image and Vision Computing*, 26(7):871–877, 2008. 2, 8

[41] Peter Sturm. On focal length calibration from two views. In *Proceedings of the 2001 IEEE Computer Society Conference on Computer Vision and Pattern Recognition. CVPR 2001*, volume 2, pages 145–150. IEEE, 2001. 2, 8

[42] Peter Sturm, ZL Cheng, Peter CY Chen, and Aun Neow Poo. Focal length calibration from two views: method and analysis of singular cases. *Computer Vision and Image Understanding*, 99(1):58–95, 2005. 2

[43] Jiaming Sun, Zehong Shen, Yuang Wang, Hujun Bao, and Xiaowei Zhou. Loftr: Detector-free local feature matching with transformers. In *Proceedings of the IEEE/CVF conference on computer vision and pattern recognition*, pages 8922–8931, 2021. 7

[44] Magdalena Urbanek, Radu Horaud, and Peter Sturm. Combining off-and on-line calibration of a digital camera. In *Proceedings Third International Conference on 3-D Digital Imaging and Modeling*, pages 99–106. IEEE, 2001. 2

[45] Bin Xu and Zhenzhong Chen. Multi-level fusion based 3d object detection from monocular images. In *Proceedings of the IEEE conference on computer vision and pattern recognition*, pages 2345–2353, 2018. 1

[46] Zhengyou Zhang. A flexible new technique for camera calibration. *IEEE Transactions on pattern analysis and machine intelligence*, 22(11):1330–1334, 2000. 1

[47] Zichao Zhang, Torsten Sattler, and Davide Scaramuzza. Reference pose generation for long-term visual localization via learned features and view synthesis. *International Journal of Computer Vision*, 129:821–844, 2021. 2, 7, 8

Supplementary Material

1. Outline

Our supplementary material provides additional details on the method presented in Section 3 in the main paper, and promised experiments that support the material from the main paper. In Section 2, we summarize our algorithm for estimating focal lengths from a given fundamental matrix \mathbf{F} . In Section 3 we provide more details on the real focal length checking (RFC) described in Section 3.2 of the main paper along with additional experiments. To supplement the results presented in Section 5 of the main paper, we present experiments on real-world data incorporating different RANSAC variants and matches in Section 4. Additionally, in Section 5 we provide both synthetic and real-world experiments for the case when the focal lengths of the two cameras are equal.

2. Algorithm

The complete algorithm for our method for estimating focal lengths from a given fundamental matrix \mathbf{F} is presented in Algorithm 1. The algorithm solves the constrained optimization problem described in Section 3 of the main paper by searching for stationary points of the Lagrange multiplier (Equation (3) in the main paper). In each iteration, this algorithm solves a system of two equations of degree four in two unknowns using the Gröbner basis method [14] (for more details see the main paper).

In each iteration, the obtained solutions satisfy the Kruppa equations $\kappa_1 = 0$ and $\kappa_2 = 0$. This means that for the input fundamental matrix \mathbf{F} and the estimated calibration matrices \mathbf{K}_1 and \mathbf{K}_2 , the matrix $\mathbf{K}_1^\top \mathbf{F} \mathbf{K}_2$ is a valid essential matrix in each iteration.

For the case of equal focal lengths, *i.e.*, $f_1 = f_2$, the algorithm has the same structure as Algorithm 1 and it also solves the system of two equations of degree four in two unknowns. The only difference is that in each step $i = 1$.

3. Real Focal Length Checking

In this section, we provide further details on the real focal length checking (RFC) described in section 3.2 of the main paper.

We implemented RFC by utilizing formula (1) for computing the focal length from the elements of the given fun-

Algorithm 1

Input: Fundamental matrix \mathbf{F} ,
 Priors $f_i^p, \mathbf{c}_i^p, i = 1, 2$,
 $\epsilon_1, maxiter$
Output: $(f_1^*, f_2^*, \mathbf{c}_1^*, \mathbf{c}_2^*)$

```

1: found  $\leftarrow 0$ ,  $k \leftarrow 1$ 
2:  $f_i^0 \leftarrow f_i^p, \mathbf{c}_i^0 \leftarrow \mathbf{c}_i^p, i = 1, 2$ 
3:  $s^0 \leftarrow \langle f_1^0, f_2^0, \mathbf{c}_1^0, \mathbf{c}_2^0 \rangle$ 
4: while (not found) and ( $k \leq maxiter$ ) do
5:    $\Delta f_i \leftarrow \frac{1}{w_i^f} (\lambda_1 \frac{\partial \kappa_1}{\partial f_i} (s^{k-1}) + \lambda_2 \frac{\partial \kappa_2}{\partial f_i} (s^{k-1}))$ 
6:    $\Delta \mathbf{c}_i \leftarrow \frac{1}{w_i^c} (\lambda_1 (\frac{\partial \kappa_1}{\partial \mathbf{c}_i} (s^{k-1}))^\top + \lambda_2 (\frac{\partial \kappa_2}{\partial \mathbf{c}_i} (s^{k-1}))^\top)$ 
7:    $\lambda_1^k, \lambda_2^k \leftarrow$  The solution to two equations  $\kappa_1^k = 0$  and  

 $\kappa_2^k = 0$ , which among all 16 solutions minimizes  

 $|\lambda_1| + |\lambda_2|$ 
8:    $\Delta f_i^k \leftarrow \Delta f_i(\lambda_1^k, \lambda_2^k), i = 1, 2$ 
9:    $\Delta \mathbf{c}_i^k \leftarrow \Delta \mathbf{c}_i(\lambda_1^k, \lambda_2^k), i = 1, 2$ 
10:   $e^k \leftarrow \sum_{i=1,2} w_i^f (\Delta f_i^k)^2 + w_i^c (\Delta \mathbf{c}_i^k)^\top \Delta \mathbf{c}_i^k$ 
11:   $f_i^k \leftarrow \Delta f_i^k + f_i^p, \mathbf{c}_i^k = \Delta \mathbf{c}_i^k + \mathbf{c}_i^p, i = 1, 2$ 
12:  if ( $k > 1$  and  $\frac{|e^k - e^{k-1}|}{e^k} < \epsilon_1$ ) then
13:     $\langle f_1, f_2, \mathbf{c}_1, \mathbf{c}_2 \rangle \leftarrow \langle f_1^k, f_2^k, \mathbf{c}_1^k, \mathbf{c}_2^k \rangle$ 
14:    found  $\leftarrow 1$ 
15:  else
16:     $k \leftarrow k + 1$ 
17:  end if
18: end while
19: if not found then
20:    $\langle f_1, f_2, \mathbf{c}_1, \mathbf{c}_2 \rangle \leftarrow \langle f_1^{k-1}, f_2^{k-1}, \mathbf{c}_1^{k-1}, \mathbf{c}_2^{k-1} \rangle$ 
21: end if

```

damental matrix \mathbf{F} . This formula was presented in [18]. To obtain f_2^2 , the same formula can be used with \mathbf{F} transposed. In the code we only check the signs of the numerator and denominator to conclude whether $f_i^2 > 0$. The check thus uses only computationally efficient operations. Note that the formula (1) assumes that both principal points lie at the origin of the camera coordinate system. When the positions of both principal points are known but different from the origin, the fundamental matrix can be easily transformed so that the principal points lie at the origin [22].

$$f_1^2 = \frac{-\mathbf{F}_{33}(\mathbf{F}_{12}\mathbf{F}_{13}\mathbf{F}_{33} - \mathbf{F}_{13}^2\mathbf{F}_{32} + \mathbf{F}_{22}\mathbf{F}_{23}\mathbf{F}_{33} - \mathbf{F}_{23}^2\mathbf{F}_{32})}{\mathbf{F}_{11}\mathbf{F}_{12}\mathbf{F}_{31}\mathbf{F}_{33} - \mathbf{F}_{11}\mathbf{F}_{13}\mathbf{F}_{31}\mathbf{F}_{32} + \mathbf{F}_{12}^2\mathbf{F}_{32}\mathbf{F}_{33} - \mathbf{F}_{12}\mathbf{F}_{13}\mathbf{F}_{32}^2 + \mathbf{F}_{21}\mathbf{F}_{22}\mathbf{F}_{31}\mathbf{F}_{33} - \mathbf{F}_{21}\mathbf{F}_{23}\mathbf{F}_{31}\mathbf{F}_{32} + \mathbf{F}_{22}^2\mathbf{F}_{32}\mathbf{F}_{33} - \mathbf{F}_{22}\mathbf{F}_{23}\mathbf{F}_{32}^2} \quad (1)$$

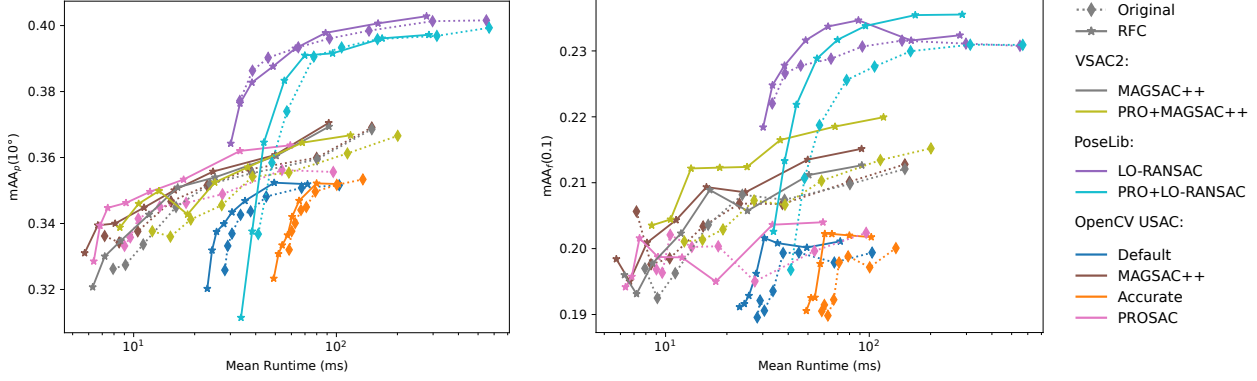


Figure 1. Figure shows the pose (left) and focal length (right) mean average accuracy on the Phototourism dataset [13] obtained after decomposing fundamental matrices with the Bougnoux formula [3]. To check the speed-accuracy trade-off we vary the total number of iterations of various RANSAC implementations with and without performing RFC.

We implemented RFC into three state-of-the-art libraries for fundamental matrix estimation: OpenCV [4], VSAC [12] and PoseLib [15]. The implementations are modular, and thus allow us to test RFC with different types of RANSACs even within a single library.

In OpenCV we test four configurations:

- Default - LO-RANSAC [6],
- Accurate - LO-RANSAC [6] + GC-RANSAC [1],
- MAGSAC++ [2],
- PROSAC [5].

In VSAC we test the two configurations which both use MAGSAC++, one with PROSAC and one without it. All of the OpenCV and VSAC variants also utilize the oriented epipolar constraint [7] and DEGENSAC [8] degeneracy checks and SPRT verification [17]. In PoseLib we test the default configuration implementing LO-RANSAC with and without PROSAC. The modified versions of these libraries will be made available online.¹

3.1. Speed-accuracy Trade-off

In Fig. 3 of the main paper we have shown that employing RFC within different implementations of RANSAC leads to improvement in both the speed of computation as well as the estimated poses when using the ground truth focal lengths to decompose the obtained fundamental matrices. Here, we show that this is also generally the case when decomposing the fundamental matrices using the Bougnoux formula [3] (Fig. 1) and our method (Fig. 2). We show that the accuracy and computation speed improvements can, in

general, be observed both in terms of pose accuracy and estimated focal length accuracy.

We measured the run-time of each RANSAC variant on the Phototourism dataset [13] using LoFTR [23] correspondences. We set the epipolar threshold for all variants to 3px. We ran the evaluation on the 200 sample pairs from each of the 12 test scenes of Phototourism. The pairs were randomly selected based on the co-visibility criteria as outlined in [13]. We let each of the RANSAC variants run for 50, 100, 500, 1000, 2000, 5000 and 10000 iterations. We prevented early termination by setting the confidence parameter to 1.0 for all methods. All tests were performed on an Intel i7-11800H CPU. For comparison, we averaged the wall-clock runtimes over all of the evaluated samples.

4. Additional Real-world Experiments

In this section, we present additional results on the Phototourism [13] and Aachen Day-Night v1.1 [24] datasets, as promised in Section 5 in the main paper. We test how the compared methods perform when we use different robust estimators of the fundamental matrix as well as different matches.

In the main paper in Table 1 and Figs. 4a and 4b we present experiments with LoFTR [23] matches. We also performed experiments using the combination of the SuperPoint [9] keypoint detector along with the SuperGlue [19] matching network to obtain matches in images. Before inference, we resize the images such that the larger dimension of the image is 2048 pixels. Note that the memory requirements of the SuperGlue network depend on the number of detected keypoints. This led to insufficient GPU memory

¹https://github.com/kocurvik/robust_self_calibration

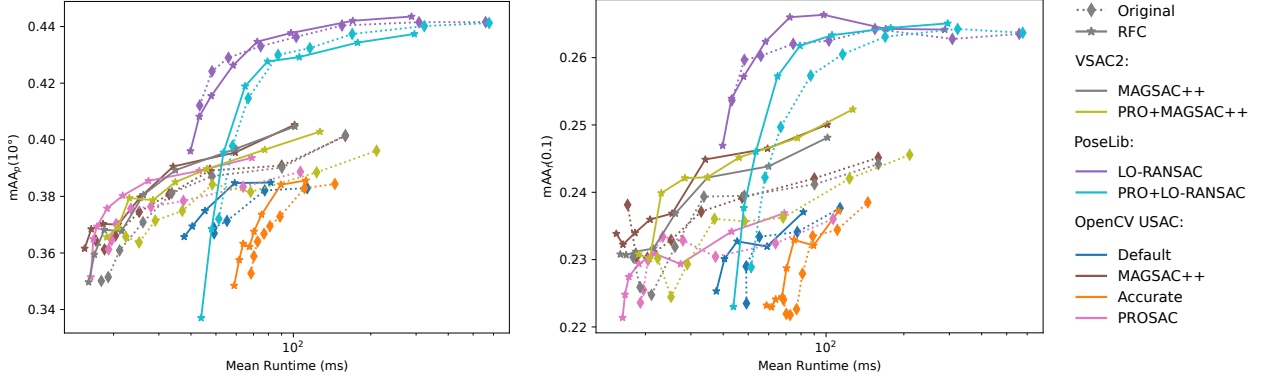


Figure 2. Figure shows the pose (left) and focal length (right) mean average accuracy on the Phototourism dataset [13] obtained after decomposing fundamental matrices with our method. To check the speed-accuracy trade-off we vary the total number of iterations of various RANSAC implementations with and without performing RFC.

Method	RFC	Phototourism [13]						Aachen Day-Night v1.1 [24]					
		Median p_{err}	mAA _p		Median f_{err}	mAA _f		Median p_{err}	mAA _p		Median f_{err}	mAA _f	
			10°	20°		0.1	0.2		10°	20°		0.1	0.2
Ours	✓	5.60° 5.59°	44.06 44.13	59.04 59.31	0.137 0.136	25.78 25.80	39.50 39.59	9.07° 8.85°	29.07 29.11	47.05 47.96	0.190 0.190	14.17	27.43
Hartley [11]	✓	8.74° 8.71°	31.45 31.52	48.38 48.62	0.209 0.207	13.88 14.10	26.20 26.51	11.87° 11.69°	21.49 21.80	39.64 40.77	0.263 0.249	6.54 6.87	14.87 15.54
Fetzer [10]	✓	8.10° 7.94°	36.06 36.23	49.88 50.24	0.201 0.194	21.34 21.43	32.58 32.91	12.87° 11.21°	24.46 25.57	38.96 41.70	0.244 0.216	11.87 13.00	23.64 25.32
Bougnoux [3]	✓	6.63° 6.63°	40.41 40.45	55.70 55.62	0.185 0.179	22.49 22.65	34.02 34.49	10.18° 9.58°	27.42 27.93	45.47 46.49	0.237 0.213	11.78 12.92	23.90 25.58
Prior	✓	11.03° 11.01°	22.78 22.81	42.42 42.53	0.206 0.206	9.52 9.52	22.75 22.75	13.08° 12.52°	17.15 17.63	37.28 38.71	0.195 0.195	4.43 4.43	10.02 10.02
GT intrinsics	✓	2.31° 2.34°	63.80 63.88	73.86 74.05	—	—	—	4.19° 4.02°	52.05 53.21	63.87 65.89	—	—	—

Table 1. Median errors for poses (p_{err}) and focal lengths (f_i^{err}) and mean average accuracy scores for poses (mAA_p) and estimated focal lengths (mAA_f) on 12 scenes from the Phototourism dataset [13] and the Aachen Day-Night v1.1 dataset [24]. Matches were produced using LoFTR [23] and the fundamental matrices were estimated using the PoseLib [15] implementation of LO-RANSAC [6]. RFC denotes real focal length checking.

Method	RFC	Phototourism [13]						Aachen Day-Night v1.1 [24]					
		Median p_{err}	mAA _p		Median f_{err}	mAA _f		Median p_{err}	mAA _p		Median f_{err}	mAA _f	
			10°	20°		0.1	0.2		10°	20°		0.1	0.2
Ours	✓	6.45° 6.29°	40.28 40.71	57.09 57.48	0.140 0.137	24.41 24.72	38.59 39.10	9.91° 8.85°	26.07 27.79	45.76 47.91	0.203 0.195	12.80 13.05	25.13 25.83
Hartley [11]	✓	8.90° 8.78°	30.83 31.00	48.49 48.60	0.206 0.206	13.45 13.61	26.09 26.24	12.01° 11.40°	20.13 21.13	39.20 40.68	0.259 0.247	6.97 7.74	15.56 16.87
Fetzer [10]	✓	9.15° 8.80°	32.51 33.08	47.94 48.72	0.197 0.191	20.40 20.58	32.00 32.38	12.42° 11.17°	22.23 23.20	38.76 41.28	0.237 0.219	11.83 12.92	23.22 24.82
Bougnoux [3]	✓	7.53° 7.40°	36.48 36.77	53.43 53.59	0.185 0.176	21.13 21.46	33.10 33.73	10.20° 9.88°	25.75 25.92	44.86 45.13	0.235 0.222	12.21 13.01	23.60 24.90
Prior	✓	10.74° 10.68°	23.37 23.60	43.46 43.62	0.205 0.205	9.52 9.52	22.77 22.77	11.93° 11.48°	17.82 18.62	39.47 40.83	0.280 0.280	7.20 7.20	13.42 13.42
GT intrinsics	✓	3.02° 3.00°	59.58 59.78	72.07 72.27	—	—	—	4.77° 4.50°	48.98 50.55	64.11 65.50	—	—	—

Table 2. Median errors for poses (p_{err}) and focal lengths (f_i^{err}) and mean average accuracy scores for poses (mAA_p) and estimated focal lengths (mAA_f) on 12 scenes from the Phototourism dataset [13] and the Aachen Day-Night v1.1 dataset [24]. Matches were produced using SuperPoint [9] in combination with SuperGlue [19]. The OpenCV [4] implementation of MAGSAC++ [2] was used to estimate the fundamental matrices. RFC denotes the real focal length checking.

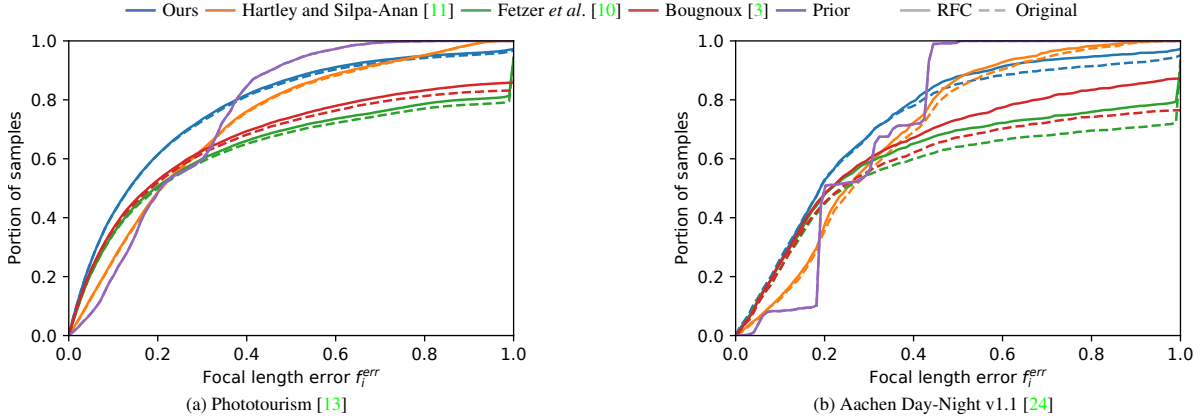


Figure 3. Plots showing the portion of samples for which the estimated focal lengths were below a given f_i^{err} threshold. Both cameras are assumed to have different unknown focal lengths. To obtain correspondences we used LoFTR [23]. We produced the fundamental matrices using the PoseLib [15] implementation of LO-RANSAC [6].

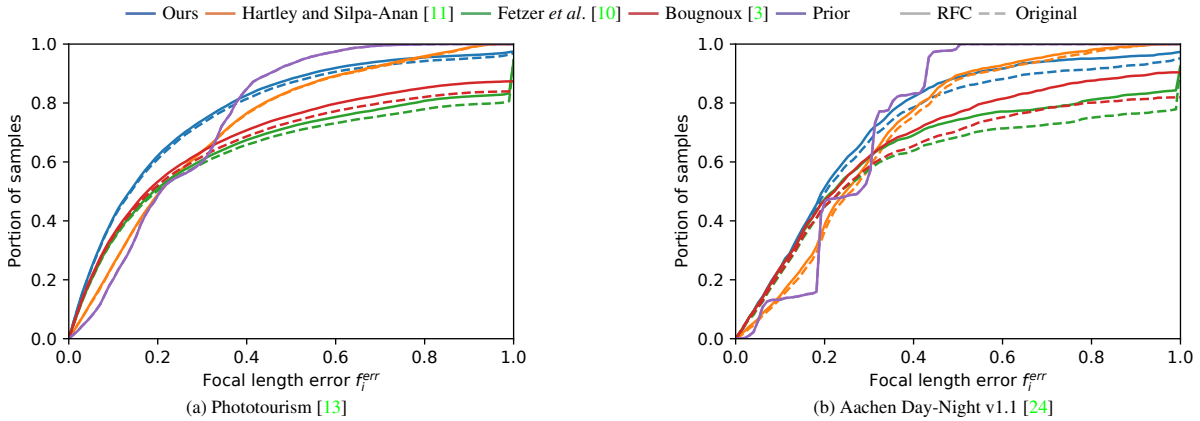


Figure 4. Plots showing the portion of samples for which the estimated focal lengths were below a given f_i^{err} threshold. Both cameras are assumed to have different unknown focal lengths. To obtain correspondences we used SuperPoint [9] and SuperGlue [19]. We produced the fundamental matrices using the OpenCV [4] implementation of MAGSAC++ [2]

for some of the pairs in both datasets. We therefore skip such pairs, but add additional pairs to keep 1000 sample pairs per each scene.

To estimate the fundamental matrices in the main paper we use MAGSAC++ [2] as implemented in OpenCV [4]. We have set the epipolar threshold to 3 px using the validation set. Here we also include experiments using LO-RANSAC [6] implemented in the PoseLib library [15]. We also use it with the epipolar threshold set to 3 px based on performance on the validation set. We set the number of iterations to 10000.

Table 1 and Fig. 3 show the results on both datasets for the combination of LoFTR matches with PoseLib LO-RANSAC. We present the results for the combination of SuperPoint, SuperGlue and MAGSAC++ in Table 2 and Fig. 4. The results for the same matches in combination with PoseLib LO-RANSAC are shown in Table 3 and Fig. 5.

These results show that our method outperforms competing approaches when different RANSAC and matching methods are considered in the fundamental matrix estimation pipeline. The results also show that performing the real focal length check (RFC) generally leads to better accuracy in both the estimated poses and focal lengths across the compared methods.

5. Cameras with Equal Focal Lengths

In this section, we present additional details and experiments for the case when the focal lengths of the two cameras are assumed to be equal. We use the algorithm modified for this scenario as described in Section 2.

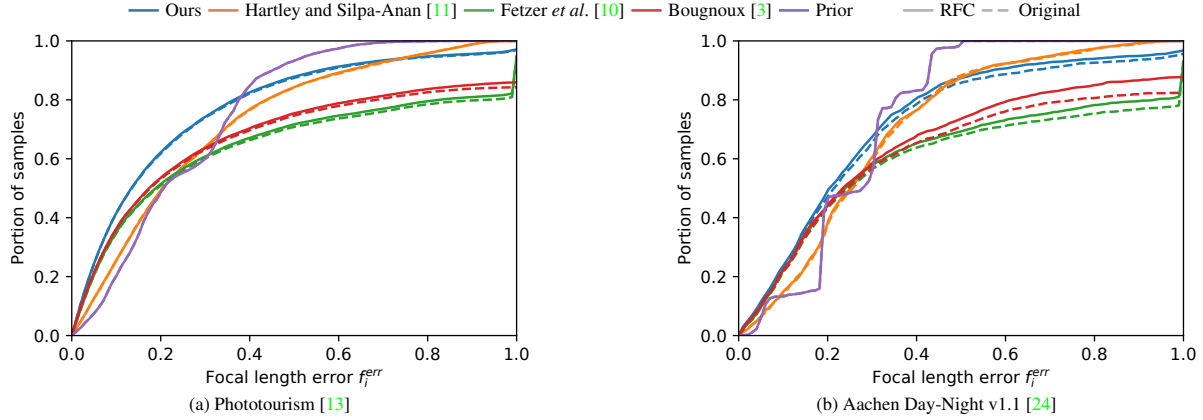


Figure 5. Plots showing the portion of samples for which the estimated focal lengths were below a given f_i^{err} threshold. Both cameras are assumed to have different unknown focal lengths. To obtain correspondences we used SuperPoint [9] in combination with SuperGlue [19]. We produced the fundamental matrices using the PoseLib [15] implementation of LO-RANSAC [6].

Method	RFC	Phototourism [13]						Aachen Day-Night v1.1 [24]					
		Median p_{err}	mAA _p		Median f_{err}	mAA _f		Median p_{err}	mAA _p		Median f_{err}	mAA _f	
			10°	20°		0.1	0.2		10°	20°		0.1	0.2
Ours	✓	5.90° 5.87°	42.85 42.87	59.35 59.43	0.135 0.134	25.21 25.25	39.44 39.59	10.01° 9.57°	26.46 27.27	46.13 47.23	0.215 0.205	12.19 12.86	24.43 25.20
Hartley [11]	✓	8.45° 8.51°	31.92 31.87	49.55 49.57	0.205 0.204	13.76 13.86	26.45 26.45	11.82° 11.46°	21.09 21.42	40.07 40.84	0.256 0.251	7.38 7.58	16.25 16.50
Fetzer [10]	✓	8.35° 8.35°	34.65 34.66	49.71 49.91	0.193 0.188	21.14 21.30	32.86 33.12	12.57° 12.45°	22.09 22.39	38.40 39.04	0.247 0.240	11.05 11.29	22.43 22.93
Bougnoux [3]	✓	6.90° 6.93°	38.88 38.76	55.51 55.35	0.177 0.174	22.06 22.14	34.22 34.40	10.20° 10.13°	25.49 25.55	44.67 44.48	0.243 0.235	11.42 11.78	22.75 23.40
Prior	✓	10.64° 10.68°	23.60 23.57	43.80 43.78	0.205 0.205	9.52 9.52	22.77 22.77	11.70° 11.57°	17.88 17.97	40.24 40.45	0.280 0.280	7.20 7.20	13.42 13.42
GT intrinsics	✓	2.66° 2.67°	62.56 62.62	74.50 74.54	— —	— —	— —	4.32° 4.26°	50.83 51.35	65.57 66.03	— —	— —	— —

Table 3. Median errors for poses (p_{err}) and focal lengths (f_i^{err}) and mean average accuracy scores for poses (mAA_p) and estimated focal lengths (mAA_f) on 12 scenes from the Phototourism dataset [13] and the Aachen Day-Night v1.1 dataset [24]. Matches were produced using SuperPoint [9] in combination with SuperGlue [19]. The PoseLib [15] implementation of LO-RANSAC [6] was used to estimate the fundamental matrices. RFC denotes the real focal length checking.

5.1. Synthetic Experiments

We perform the same synthetic experiments as for the case of two cameras with unknown but different focal lengths (cf. Section 4 in the main paper). We use the same notation for camera configurations and added noise. We note that the configuration of $\mathcal{C}(0^\circ, 0)$ has the two principal axes meeting at a point equidistant from both camera centers. Thus it is a degenerate configuration leading to a generic singularity in the Kruppa equations [16] when the focal lengths are considered equal.

Convergence: Figures 6a and 6b show convergence rates in non-degenerate and degenerate configurations respectively. The method converges in the majority of cases in a few iterations, even when strict thresholds are considered.

The algorithm also converges within 50 iterations for the majority of the cases on real data from the ETH3D Multi-view dataset [20] as shown in Fig. 6c. Therefore, we set the maximum number of iterations to 50 in further experiments.

Accuracy of the Estimated Focal Length: For comparison, we use the method by Fetzer *et al.* to optimize for a single focal length for both cameras. Instead of the Bougnoux formula [3], we use the formula proposed by Sturm [22] that is specific to the case of equal focal lengths. We use Hartley and Silpa-Anan's method [11] as usual, but on output we average the two focal lengths produced. We have also implemented Hartley and Silpa-Anan's method to estimate a single focal length while utilizing the Sturm formula in the iterative optimization loop, but we found it to produce less

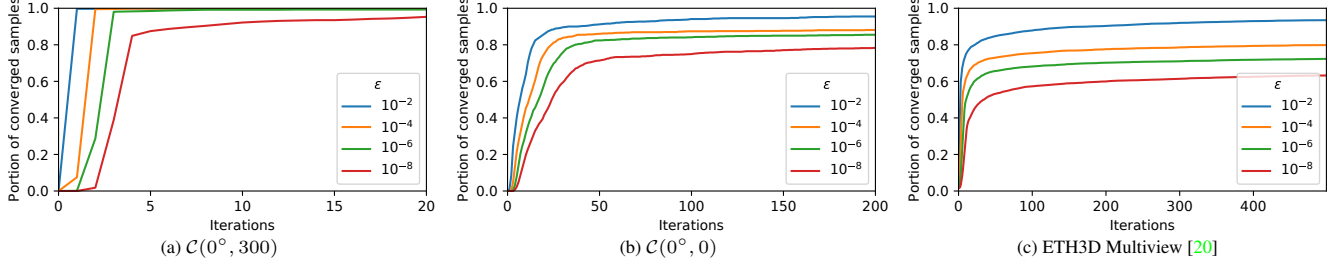


Figure 6. Plots showing portion of samples for which our algorithm would converge given a threshold for the relative change of errors in successive iterations $\frac{|e^n - e^{n-1}|}{e^n} < \epsilon$. For synthetic experiments (a) and (b) we generated 1000 samples with added noise ($\sigma_n = 1$, $\sigma_p = 10$). We set the prior as $f^p = 660$. For (c) we used the ETH3D Multiview dataset [20].

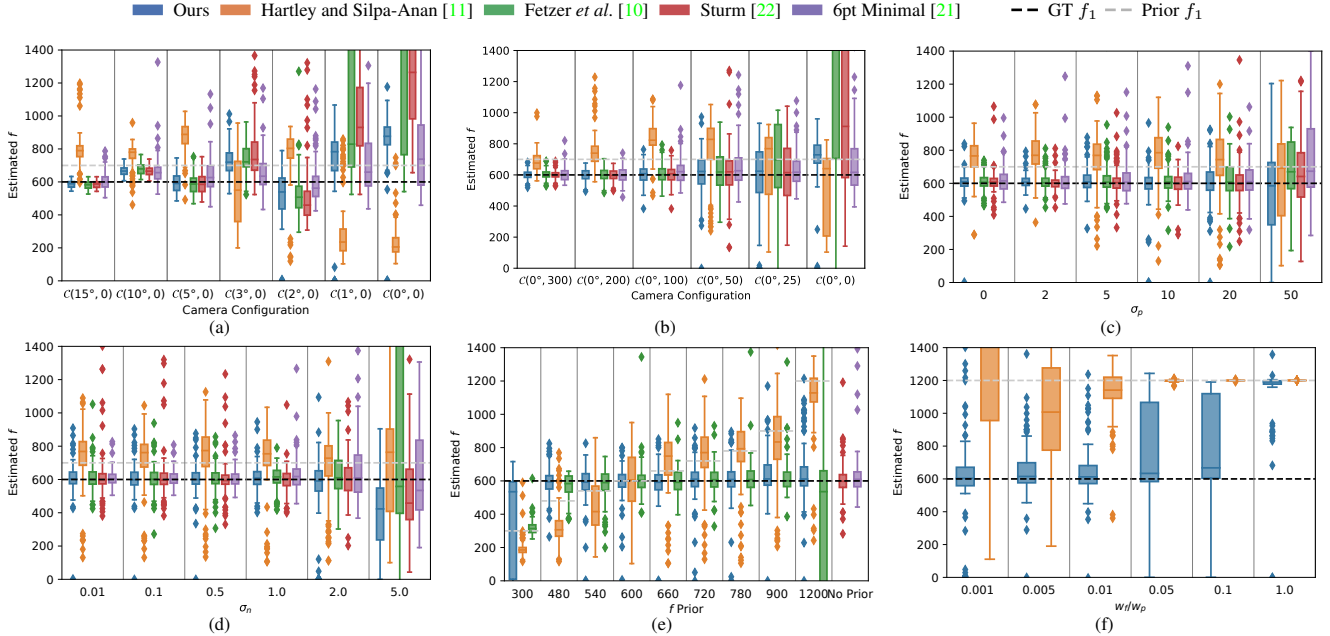


Figure 7. Synthetic experiments: Box plots for the estimated focal length equal for the two cameras. Comparison of the methods as (a, b) the camera configuration approaches the degenerate configuration, (c) we vary the standard deviation σ_p of the error of the principal point, (d) we vary the noise added to the projected points, (e) we vary the prior for f , (f) we vary the relative weights of the focal length and principal point priors. We use priors $f^p = 700$ for (a, b, c, d), $f^p = 1200$ for (f), $\sigma_n = 1$ for (a, b, c, e, f), $\sigma_p = 10$ for (a, b, d, e, f). For (c, d, e, f) we randomly sample the configuration $\mathcal{C}(\theta, y)$ with $\theta \in [-15^\circ, 15^\circ]$ and $y \in [-200, 200]$.

stable results than those for the selected approach.

We also evaluate the minimal 6-point algorithm [21] implemented within LO-RANSAC [6, 15]. We set the number of iterations to 10000 and the epipolar threshold to 1 px.

Fig. 7 shows the results of the synthetic experiments. We observe a similar behavior as in synthetic experiments for the case of different focal lengths presented in the main paper (*cf.* Section 4). However, there are some differences that are specific for the equal focal length case and different methods tested in this case. Hartley and Silpa-Anan's iterative method performs poorly in this scenario. The Sturm's method for equal focal lengths is more stable than the Bougnoux formula for the general case. The method by Fetzer *et al.* provides results similar to those of the Sturm's

formula, but it is less stable when bad initialization is used or when the cameras are near the degenerate configuration. The 6-point minimal algorithm provides stable results even in proximity of the degenerate configuration. Our method performs on par with the minimal 6-point algorithm, thus providing a viable alternative.

5.2. Real-world Experiments

In the main paper (*cf.* Sec 5, Table 3), we have presented a comparison of various methods on the ETH3D Multiview dataset [20]. Here, we present additional experiments which include evaluation of the compared methods when RFC is used. We also include experiments using a different RANSAC variant. We use LoFTR [23] to obtain matches.

Method	RFC	PoseLib LO-RANSAC [6,15]						OpenCV MAGSAC++ [2,4]					
		Median p_{err}	mAA _p		Median f_{err}	mAA _f		Median p_{err}	mAA _p		Median f_{err}	mAA _f	
			10°	20°		0.1	0.2		10°	20°		0.1	0.2
Ours	✓	15.20°	17.69	33.66	0.240	14.92	25.92	16.51°	16.70	32.24	0.244	13.69	25.01
		14.84°	18.07	34.26	0.225	15.35	26.79	15.70°	16.97	33.01	0.226	14.58	26.25
Hartley [11]	✓	21.09°	12.41	24.40	0.523	0.53	1.26	21.52°	12.38	24.26	0.523	0.46	1.12
		21.11°	12.24	24.19	0.522	0.43	1.01	21.70°	12.34	24.14	0.523	0.58	1.16
Fetzer [10]	✓	23.18°	18.56	29.04	0.999	7.54	12.29	23.93°	17.64	27.93	0.999	6.86	11.64
		20.27°	17.86	29.65	0.747	8.39	13.92	19.72°	17.89	30.08	0.741	8.28	13.90
Sturm [22]	✓	16.40°	21.82	34.93	0.511	11.38	19.08	17.98°	20.64	33.30	0.524	10.78	18.46
		16.42°	20.61	34.26	0.342	12.98	22.15	17.18°	19.36	33.01	0.331	12.82	21.99
Minimal 6pt [21]	—	36.18°	16.42	25.74	0.239	15.04	25.89	36.18°	16.42	25.74	0.239	15.04	25.89
Prior	✓	24.38°	11.25	20.80	0.528	0.00	0.00	24.60°	11.24	20.92	0.528	0.00	0.00
		24.53°	11.11	20.74	0.528	0.00	0.00	24.45°	11.28	21.07	0.528	0.00	0.0
GT intrinsics	✓	5.95°	43.20	55.72	—	—	—	6.40°	41.73	54.16	—	—	—
		5.87°	43.30	56.00	—	—	—	6.41°	41.54	54.57	—	—	—

Table 4. Median errors for poses (p_{err}) and focal lengths (f_{err}) and mean average accuracy scores for poses (mAA_p) and estimated focal lengths (mAA_f) on the ETH3D Multiview dataset [20]. LoFTR [23] was used to produce matches. To estimate the fundamental matrices we used two different estimators: PoseLib LO-RANSAC [6, 15] and OpenCV MAGSAC++ [2, 4]. The minimal solver was implemented within the PoseLib LO-RANSAC framework. RFC denotes real focal length checking.

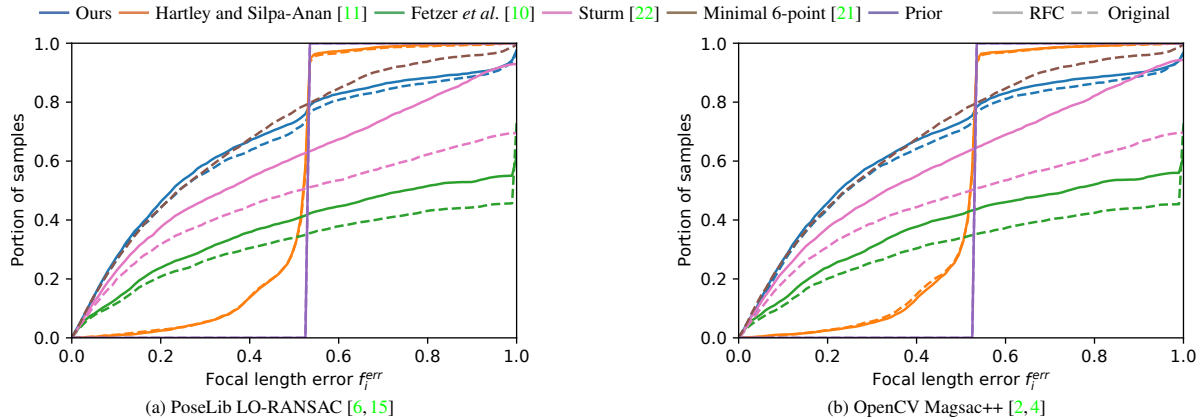


Figure 8. Plots showing the portion of samples for which the estimated focal lengths were below a given f_{err} threshold on the ETH 3D Multiview dataset [20]. The focal lengths for the two cameras are assumed to be equal. To obtain correspondences we used LoFTR [23]. We produced the fundamental matrices using (a) the PoseLib [15] implementation of LO-RANSAC [6] (b) the OpenCV [4] implementation of MAGSAC++ [2].

We matched all pairs of images that had co-visibility factor [13] greater than 0.1. Prior to inference, we resized the images so that the larger size is 1024 px. We estimated the fundamental matrices using LO-RANSAC [6] implemented in PoseLib [15] and MAGSAC++ [2] implemented in OpenCV [4].

The results show that using our method in conjunction with RFC leads to good accuracy in terms of both the estimated poses and focal lengths. In comparison, the Sturm’s method achieves the highest mAA_p scores, but performs poorly with respect to focal length accuracy. On the other hand, the minimal solver shows good results in terms of the estimated focal lengths but shows weak results when it comes to pose accuracy. Our method is thus a viable alter-

native to other existing approaches, when both cameras are assumed to have equal focal lengths.

References

- [1] Daniel Barath and Jiří Matas. Graph-cut ransac. In *Proceedings of the IEEE conference on computer vision and pattern recognition*, pages 6733–6741, 2018. [12](#)
- [2] Daniel Barath, Jana Noskova, Maksym Ivashechkin, and Jiri Matas. Magsac++, a fast, reliable and accurate robust estimator. In *Proceedings of the IEEE/CVF conference on computer vision and pattern recognition*, pages 1304–1312, 2020. [12](#), [13](#), [14](#), [17](#)
- [3] Sylvain Bougnoux. From projective to euclidean space under any practical situation, a criticism of self-calibration. In *Sixth*

International Conference on Computer Vision, pages 790–796. IEEE, 1998. 12, 13, 14, 15

[4] Gary Bradski. The opencv library. *Dr. Dobb’s Journal: Software Tools for the Professional Programmer*, 25(11):120–123, 2000. 12, 13, 14, 17

[5] Ondrej Chum and Jiri Matas. Matching with prosac—progressive sample consensus. In *2005 IEEE computer society conference on computer vision and pattern recognition (CVPR’05)*, volume 1, pages 220–226. IEEE, 2005. 12

[6] Ondřej Chum, Jiří Matas, and Josef Kittler. Locally optimized ransac. In *Pattern Recognition: 25th DAGM Symposium, Magdeburg, Germany, September 10-12, 2003. Proceedings 25*, pages 236–243. Springer, 2003. 12, 13, 14, 15, 16, 17

[7] Ondrej Chum, Tomás Werner, and Jiri Matas. Epipolar geometry estimation via ransac benefits from the oriented epipolar constraint. In *Proceedings of the 17th International Conference on Pattern Recognition, 2004. ICPR 2004.*, volume 1, pages 112–115. IEEE, 2004. 12

[8] Ondrej Chum, Tomas Werner, and Jiri Matas. Two-view geometry estimation unaffected by a dominant plane. In *2005 IEEE Computer Society Conference on Computer Vision and Pattern Recognition (CVPR’05)*, volume 1, pages 772–779. IEEE, 2005. 12

[9] Daniel DeTone, Tomasz Malisiewicz, and Andrew Rabinovich. Superpoint: Self-supervised interest point detection and description. In *Proceedings of the IEEE conference on computer vision and pattern recognition workshops*, pages 224–236, 2018. 12, 13, 14, 15

[10] Torben Fetzer, Gerd Reis, and Didier Stricker. Stable intrinsic auto-calibration from fundamental matrices of devices with uncorrelated camera parameters. In *Proceedings of the IEEE/CVF Winter Conference on Applications of Computer Vision*, pages 221–230, 2020. 13, 14, 15, 16, 17

[11] Richard Hartley, Chanop Silpa-Anan, et al. Reconstruction from two views using approximate calibration. In *Proc. 5th Asian Conf. Comput. Vision*, volume 1, pages 338–343, 2002. 13, 14, 15, 16, 17

[12] Maksym Ivashevchkin, Daniel Barath, and Jiří Matas. Vsac: Efficient and accurate estimator for h and f . In *Proceedings of the IEEE/CVF international conference on computer vision*, pages 15243–15252, 2021. 12

[13] Yuhe Jin, Dmytro Mishkin, Anastasiia Mishchuk, Jiri Matas, Pascal Fua, Kwang Moo Yi, and Eduard Trulls. Image matching across wide baselines: From paper to practice. *International Journal of Computer Vision*, 129(2):517–547, 2021. 12, 13, 14, 15, 17

[14] Viktor Larsson, Kalle Astrom, and Magnus Oskarsson. Efficient solvers for minimal problems by syzygy-based reduction. In *Proceedings of the IEEE Conference on Computer Vision and Pattern Recognition*, pages 820–829, 2017. 11

[15] Viktor Larsson and contributors. PoseLib - Minimal Solvers for Camera Pose Estimation, 2020. 12, 13, 14, 15, 16, 17

[16] Manolis IA Lourakis and Rachid Deriche. *Camera self-calibration using the Kruppa equations and the SVD of the fundamental matrix: The case of varying intrinsic parameters*. PhD thesis, INRIA, 2000. 15

[17] Jiri Matas and Ondrej Chum. Randomized ransac with sequential probability ratio test. In *Tenth IEEE International Conference on Computer Vision (ICCV’05) Volume 1*, volume 2, pages 1727–1732. IEEE, 2005. 12

[18] Oleh Rybkin. Robust focal length estimation. Bachelor’s thesis, Czech Technical University in Prague, 2017. 11

[19] Paul-Edouard Sarlin, Daniel DeTone, Tomasz Malisiewicz, and Andrew Rabinovich. Superglue: Learning feature matching with graph neural networks. In *Proceedings of the IEEE/CVF conference on computer vision and pattern recognition*, pages 4938–4947, 2020. 12, 13, 14, 15

[20] Thomas Schops, Johannes L Schonberger, Silvano Galliani, Torsten Sattler, Konrad Schindler, Marc Pollefeys, and Andreas Geiger. A multi-view stereo benchmark with high-resolution images and multi-camera videos. In *Proceedings of the IEEE conference on computer vision and pattern recognition*, pages 3260–3269, 2017. 15, 16, 17

[21] Henrik Stewénius, David Nistér, Fredrik Kahl, and Fredrik Schaffalitzky. A minimal solution for relative pose with unknown focal length. *Image and Vision Computing*, 26(7):871–877, 2008. 16, 17

[22] Peter Sturm. On focal length calibration from two views. In *Proceedings of the 2001 IEEE Computer Society Conference on Computer Vision and Pattern Recognition. CVPR 2001*, volume 2, pages 145–150. IEEE, 2001. 11, 15, 16, 17

[23] Jiaming Sun, Zehong Shen, Yuang Wang, Hujun Bao, and Xiaowei Zhou. Loftr: Detector-free local feature matching with transformers. In *Proceedings of the IEEE/CVF conference on computer vision and pattern recognition*, pages 8922–8931, 2021. 12, 13, 14, 16, 17

[24] Zichao Zhang, Torsten Sattler, and Davide Scaramuzza. Reference pose generation for long-term visual localization via learned features and view synthesis. *International Journal of Computer Vision*, 129:821–844, 2021. 12, 13, 14, 15